Friction **11**(1): 125–140 (2023)
https://doi.org/10.1007/s40544-021-0585-2
ISSN 2223-7690
CN 10-1237/TH
RESEARCH ARTICLE

Characterization of ultrafine particles from hardfacing coated brake rotors

Yezhe LYU[1,2,*], Ankur SINHA[3], Ulf OLOFSSON[2], Stefano GIALANELLA[3], Jens WAHLSTRÖM[1]

[1] *Department of Mechanical Engineering Sciences, Lund University, Lund SE-22100, Sweden*

[2] *Department of Machine Design, KTH Royal Institute of Technology, Stockholm SE-10044, Sweden*

[3] *Department of Industrial Engineering, University of Trento, Trento 38123, Italy*

Received: 06 October 2021 / Revised: 10 November 2021 / Accepted: 07 December 2021

Abstract: Automotive brake rotors are commonly made from gray cast iron (GCI). During usage, brake rotors are gradually worn off and periodically replaced. Currently, replaced brake rotors are mostly remelted to produce brand-new cast iron products, resulting in a relatively high energy consumption and carbon footprint into the environment. In addition, automotive brakes emit airborne particles. Some of the emitted particles are categorized as ultrafine, which are sized below 100 nm, leading to a series of health and environmental impacts. In this study, two surface treatment techniques are applied, i.e., high-velocity oxygen fuel (HVOF) and laser cladding (LC), to overlay wear-resistant coatings on conventional GCI brake rotors in order to refurbish the replaced GCI brake rotor and to avoid the remelting procedure. The two coating materials are evaluated in terms of their coefficient of friction (CoF), wear, and ultrafine particle emissions, by comparing them with a typical GCI brake rotor. The results show that the CoF of the HVOF disc is higher than those of the GCI and LC discs. Meanwhile, HVOF disc has the lowest wear rate but results in the highest wear rate on the mating brake pad material. The LC disc yields a similar wear rate as the GCI disc. The ultrafine particles from the GCI and LC discs appeared primarily in round, chunky, and flake shapes. The HVOF disc emits unique needle-shaped particles. In the ultrafine particle range, the GCI and HVOF discs generate particles that are primarily below 100 nm in the running-in period and 200 nm in the steady state. Meanwhile, the LC disc emitted particles that are primarily ~200 nm in the entire test run.

Keywords: ultrafine particle; high-velocity oxygen fuel; laser cladding; brake; particle size distribution; particle morphology

1 Introduction

The disc brake system is widely used to decelerate and stop road vehicles. This system operates in a way by pressing the brake pads against rotors and in which process dissipates the kinetic energy of the vehicles into frictional heat of the pads and rotors. Brake pad materials exhibit significant differences in terms of chemical composition, depending on the market preferences, requirements, and regulations, whereas brake rotors are typically made from gray cast iron (GCI) owing to its favorable thermal properties, high castability, and low cost. Brake pads and rotors are gradually worn off and periodically replaced. A passenger car is estimated to averagely spend 16 spare pairs of brake pads and four rotors over its entire lifetime [1]. The replaced GCI brake rotors are typically remelted with other raw materials to produce brand-new cast iron products. Considering the rather high melting point of GCI and vast volume

* Corresponding author: Yezhe LYU, E-mail: yezhe.lyu@mel.lth.se

of replaced GCI rotors worldwide, this approach results in significant energy consumption and carbon footprint into the environment. A promising strategy to refurbish the replaced GCI rotor, in contrast to the remelting approach, is to deposit a cermet coating (carbide, boride, or oxide hard metal in a metal binder) on the worn surfaces of the rotor. Different coating technologies have been attempted for this purpose, such as laser cladding (LC) [2, 3], atmospheric plasma spray [4], and high-velocity oxygen fuel (HVOF) spray [5–9]. These techniques may avoid the remelting process as well as high energy consumption and carbon footprint, at the same time increase the wear resistance of the refurbished brake rotors.

In addition to the friction and wear performance, another concern regarding the disc brake system is the airborne particulate matter (PM) emission. It is estimated that brake wear contributes up to approximately 20% by mass to the total traffic-related PM_{10} emissions (exhaust and non-exhaust) [10–12]. These particles are generally classified into different size groups that correspond to the inhalation behavior of PM into the human body, from ultrafine (UFP, i.e., particle aerodynamic diameter $D < 0.1$ μm) and fine ($PM_{2.5}$, i.e., $D < 2.5$ μm) to coarse (PM_{10}, i.e., $D < 10$ μm) particulate matter. Because the adverse health impacts of particles largely depend on their size, UFP has high deposition and penetration efficiency in the pulmonary region and other organs, thereby inducing inflammation and a series of other diseases [13, 14]. For the latest decades, great efforts have been made on fine and coarse particles emissions, regarding their size distribution, particle concentration, chemical composition, etc. [10, 15]. However, UFP emission from brake system is rarely investigated, largely due to the necessity of very advanced and costly techniques.

The purpose of this study is to investigate the particle concentration and size distribution of UFP from a HVOF, a LC and traditional GCI brake rotors, using a robust pin-on-disc (PoD) tribometer setup dedicated to airborne particle emission evaluation [16–19]. In addition, the generated UFP are collected and analyzed regarding their chemical composition and morphology to identify the mechanism of UFP generation, accumulating solid knowledge for the future improvement of hardfacing coated brake rotors.

2 Experimental

2.1 Materials

Three brake rotor materials, i.e., GCI, HVOF sprayed cermet coating, and LC Fe-based coating are PoD evaluated against a commercial low-metallic brake pad material (see below). The microstructure of the brake pad material was observed using the scanning electron microscope (SEM; JEOL JSM-IT300 InTouchScope), as shown in Fig. 1. Table 1 shows the chemical composition of the three brake rotor and the brake pad materials, either supplied by the powder manufacturer or obtained using the energy-dispersive X-ray spectroscopy (EDXS) system (XFlash 630M, Bruker). Table 2 lists some important parameters of the tested materials.

An industrial HVOF system was used to apply the commercial powder (average size 15–45 μm) (Amperit 558.074) on the GCI substrate. The spray parameters were customized in previous studies [6, 8, 20] and are as follows: kerosene flow rate, 24 L/h; oxygen flow rate, 1,000 L/min; spray distance, 400 mm. After grinding using SiC paper (220 grit), the HVOF coating exhibited a surface roughness of 1.5 μm and a thickness of 70 μm. The LC coating was obtained from a commercial Fe-based powder (average size 53–150 μm) (Höganäs Rockit 401) and was deposited on the GCI substrate using a laser system (Laserline LDF7000-40). The key parameters of the laser cladding process were as follows: laser spot size = 2 mm; laser power = 950 W;

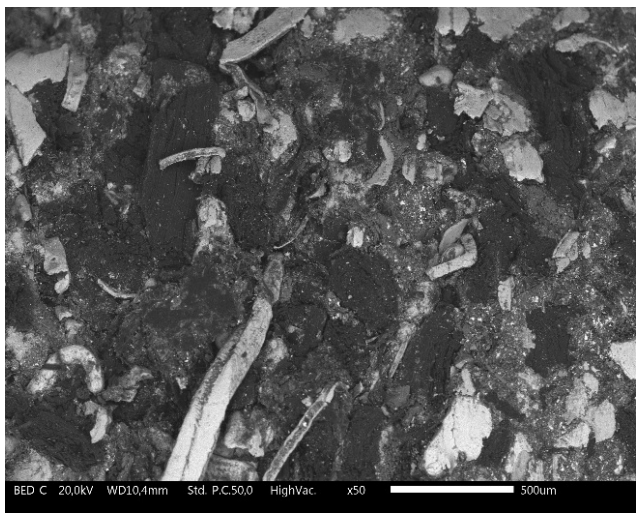

Fig. 1 Backscattered SEM image of pin microstructure.

Table 1 Chemical compositions and surface conditions of tested brake disc and pad materials. (Unit: wt%)

Element	GCI	HVOF	LC	Pad
Al	—	—	—	6.7
Ba	—	—	—	1.3
C	3.8	5.5	0.15	—
Co	—	10.0	—	—
Cr	—	4.0	18	0.8
Cu	—	—	—	21.5
Fe	Balance	0.3	Balance	14.3
Mg	—	—	—	8.4
Mn	0.65	—	—	—
Mo	—	—	0.5	—
Ni	—	—	2.5	—
O	—	—	—	19.1
S	0.05	—	—	5.2
Sb	—	—	—	7.0
Si	1.8	—	—	4.0
W	—	Balance	—	—
Zn	—	—	—	10.3
Others	—	—	—	Balance

Table 2 Important parameters of tested brake disc and pad materials.

Material	GCI	HVOF	LC	Pad
Hardness	20 HRC	1130 HV0.3	56 HRC	—
Density (g/cm^3)	7.10	15.60	13.58	2.71
Surface roughness *Ra* (μm)	0.30	1.50	0.25	Scorched

laser head travel speed = 8 mm/s; metal powder feed rate = 7 g/min. The brake pad material was manufactured into cylindrical pin samples with a testing surface measuring 10 mm in diameter, and the three brake rotor materials were manufactured into round disc samples measuring 100 mm in diameter and 8 mm thick.

2.2 PoD tribometer

Figure 2 shows an illustration of the PoD tribometer used in this study, which comprises a horizontally rotational disc and a vertically dead-loaded pin. Both the rotational speed of the motor and the weight are adjustable, thereby allowing the desired sliding speed and contact pressure between the pin and disc to be achieved. The PoD tribometer was sealed in a one-way ventilated box to eliminate the atmospheric particles. The unidirectional fan pumped room air into the ventilated box through the air inlet. The high-efficiency particulate air filter (class H13 EN 1822) filtered out the atmospheric particles, and ensured the cleanliness of the inlet air. At the air outlet, two particle measurement devices were used to monitor and collect the emitted airborne particles from the pin/disc sliding contact. The first device was a fast mobility particle sizer (FMPS; TSI Model 0391), which is capable to measure particles ranging from 5.6 to 560 nm in 32 size channels. The second device was an electrical low pressure impactor (ELPI+; DEKATI), which measures and collects particles from 6 nm to 10 μm at 14 size-resolved stages. Both the FMPS and ELPI+ have a sampling frequency of 1 Hz. In addition to the airborne particle emission, this test setup evaluates the coefficient of friction (CoF) by indirectly measuring the tangential force at the pin/disc contact. Based on the dead weight, the CoF can be calculated by dividing the tangential force by the normal force.

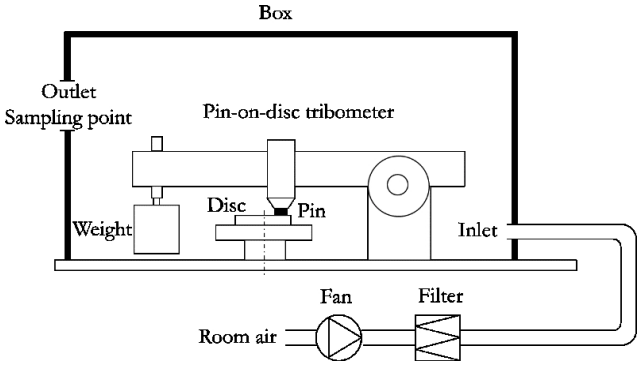

Fig. 2 Schematic illustration of test set-up. Reproduced with permission from Ref. [18], © The Authors 2019.

The wear mass loss of the tested pins and discs was measured by weighing them before and after each test run using an analytical balance (accuracy = 0.1 mg) (Sartorius ME614S). The specific wear rates of the samples were calculated with Eq. (1):

$$k = \frac{\Delta m}{\rho \cdot s \cdot F_{\mathrm{N}}} \tag{1}$$

where Δm is the mass loss of the sample; ρ is the density of the sample; s is the sliding distance; F_{N} is the normal load applied on the pin/disc contact.

This method enables the determination of the specific wear rates of both the pin and disc. This method is beneficial for the real application because the drivers usually observe the wear volume of the brake pads and rotors to order maintenance.

2.3 Test conditions

Owing to the significant variances in phase constitutions of the three brake disc materials, the resulting CoF values, obtained using the same brake pad material pressed against the three brake disc materials, are notably different. Consequently, a series of pre-tests were conducted before the formal tests commenced. The purpose of the pre-tests was to find an identical and representative friction force corresponding to the real driving practice. In real driving, the force applied on the brake pedal was dynamically adjusted to achieve the desired friction force in order to stop the car with a proper deceleration rate. After the pre-tests, the test conditions for different pin/disc combinations were obtained, as listed in Table 3. Each pin/disc combination has been tested for three repeats so that the mean value and standard deviation of the CoF, specific wear rate, and particle concentration can be obtained.

Table 3 Contact pressure and sliding speed for various material combinations.

Disc	Pin	Contact pressure (MPa)	Sliding speed (m/s)	Test duration (h)
GCI	Low-metallic	0.80	5	2
HVOF	Low-metallic	0.65	5	2
LC	Low-metallic	0.80	5	2

3 Results

3.1 CoF

Figure 3 shows the CoF time history of the three tested brake disc materials in the form of mean value (solid line) and standard deviation (shadowed area). For all the three materials, a typical running-in period is seen at the beginning of the test, where the CoF gradually increases. For the GCI and HVOF materials, the running-in period lasts for 1,500 s approximately, whilst for the LC material is only 500 s. Furthermore,

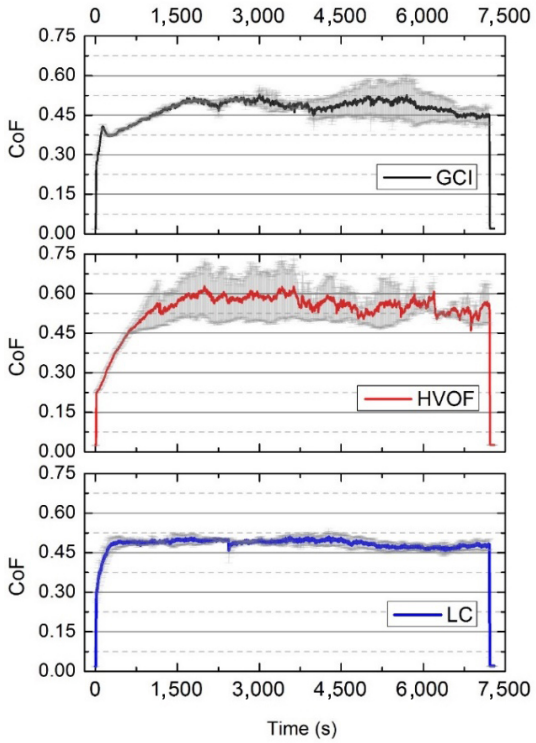

Fig. 3 CoF of three tested brake disc materials. Results are shown in terms of mean value (solid line) and standard deviation (shadowed area).

HVOF disc has a notably higher mean CoF than the GCI and LC discs. It can also be noted that the LC disc has much narrower scatter throughout the test duration than the GCI and HVOF discs.

3.2 Wear

The specific wear rates of the three brake disc materials and their mating pins are calculated according to Eq. (1) and the results are shown in Fig. 4. It can be seen that HVOF disc has the lowest wear rate among all the three brake disc materials. However, the mating pin against HVOF disc exhibits much higher wear rate than the pins tested with the GCI and LC discs. GCI and LC discs have similar wear rates, and the same result applies to wear rates of the relevant mating pins.

3.3 Particle concentration

Particle number concentration (PNC) time histories of the three brake disc materials (two repeats for each) obtained with FMPS are shown in Fig. 5. The GCI and HVOF discs have very high PNC in the running-in

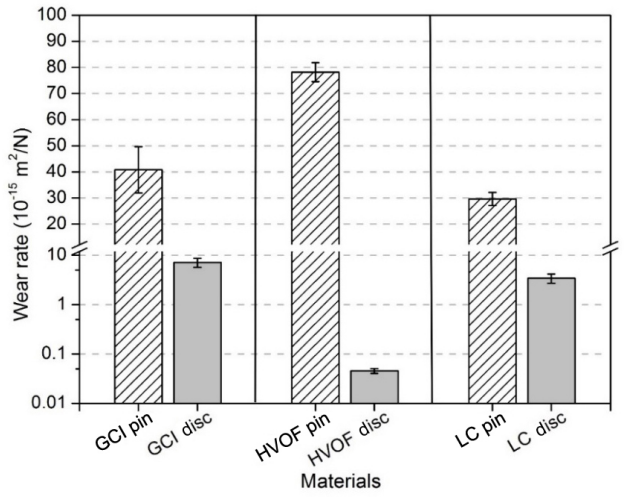

Fig. 4 Specific wear rates of tested pins and discs in terms of mean value and one standard deviation.

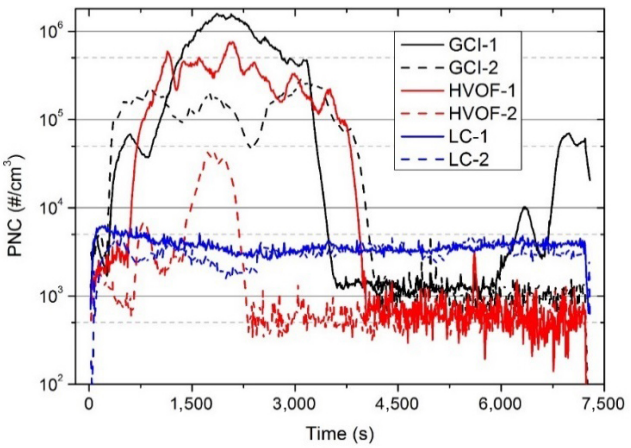

Fig. 5 Time histories of the particle number concentrations of the three brake disc materials obtained with FMPS. Two test repeats are shown for each brake disc material.

period and decreased level in the steady state. On the contrary, the LC disc has very stable PNC during the entire test run. Besides PNC, the particle mass concentrations in different ranges, i.e., PM_{10}, $PM_{2.5}$, PM_1 and $PM_{0.1}$ from the three brake disc materials are characterized by ELPI+ and presented in Fig. 6. It can be seen from the figure that PM_{10}, $PM_{2.5}$ and PM_1 of GCI and HVOF promptly reached the peak values in the beginning of the test runs, and then decreased to the steady state. However, the $PM_{0.1}$ signals of GCI and HVOF experienced prolonged running-in periods, which are likely to correspond to the PNC curves shown in Fig. 5. Similarly to the PNC result, the LC disc has very stable PM_{10}, $PM_{2.5}$, PM_1, and $PM_{0.1}$ data in the entire test run. If only the data in the steady

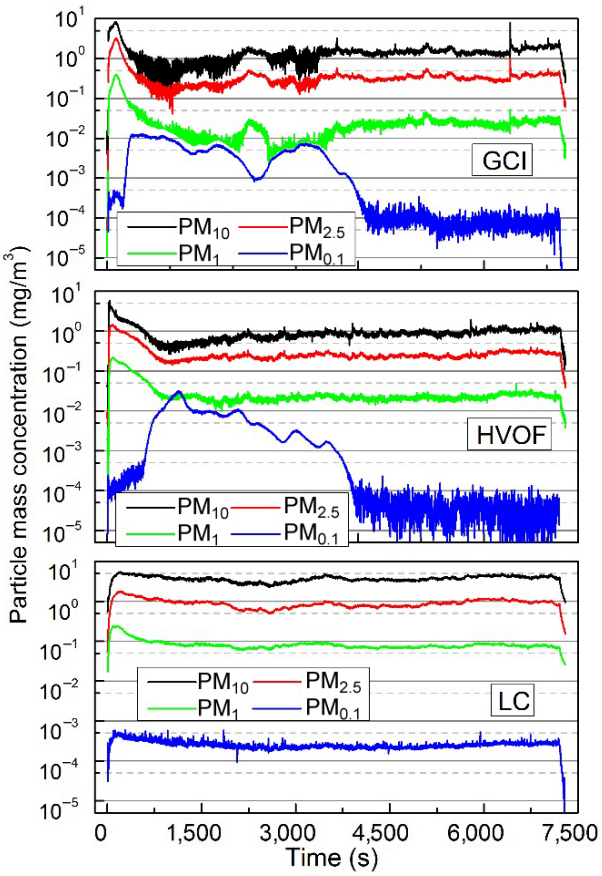

Fig. 6 Time histories of PM_{10}, $PM_{2.5}$, PM_1, and $PM_{0.1}$ of the three brake disc materials.

state are considered, LC disc has higher levels than GCI and HVOF discs in the corresponding PM_{10}, $PM_{2.5}$, PM_1, and $PM_{0.1}$ values. For the GCI and HVOF discs, the PM_{10} curve shows very different trend from $PM_{0.1}$ curve.

3.4 Particle size distribution

Figure 7 depicts the 3D contour plots of the particle generation obtained with FMPS for the three brake disc materials. The generated particles from GCI and HVOF are mainly below 100 nm whilst for LC disc are mainly above 100 nm. The particle size distributions of the three brake disc materials obtained by FMPS in the running-in period and steady state are also analyzed and shown in Fig. 8. It should be noted that FMPS only offers information on particles below 560 nm. For the particles in larger size ranges, ELPI+ was employed to characterize the particle size distributions, as presented in Fig. 9. It can be seen from Fig. 8 that in the running-in period, the emitted

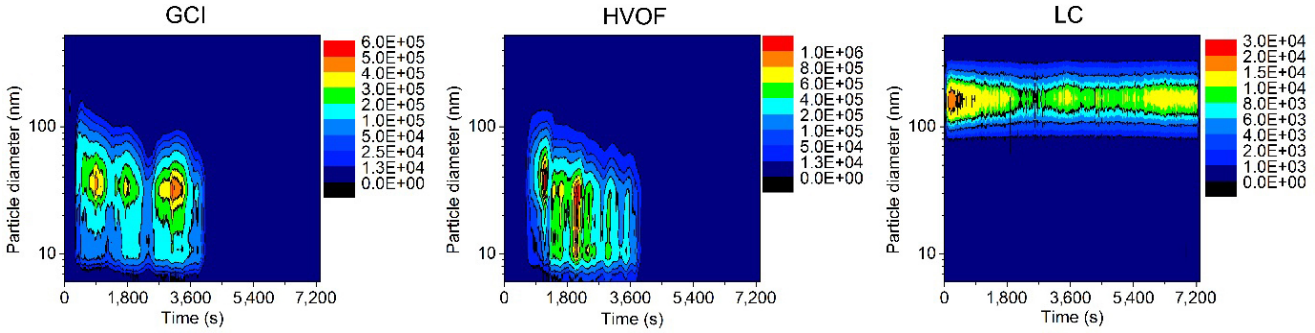

Fig. 7 3D contour plots of particle concentration dN/d(log$D$p) (#/cm^3) from the three brake disc materials.

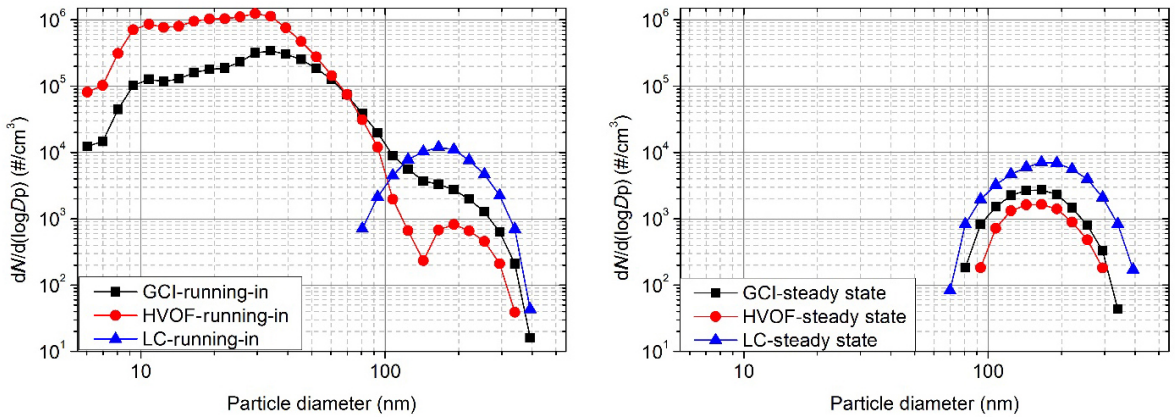

Fig. 8 Particle size distribution in the running-in and steady state obtained by FMPS.

particles from GCI and HVOF discs concentrated in the range below 100 nm whilst for the LC disc around 200 nm. This is in accordance with the results observed in the 3D contour plots shown in Fig. 7. In the steady state, all the three materials demonstrate size mode around 200 nm and LC shows the highest concentration on each particle size channel, corresponding to the results shown in Figs. 5 and 6, which indicates the highest steady-state PNC from LC disc. Figure 9 also confirms the results shown in Figs. 5–8, that the LC discs had very stable particle emission performance over the entire test run (no significant distinction between the running-in period and steady state was observed). It can also be seen in Fig. 9 that GCI and HVOF discs present a dual-modes particle size distributions in the running-in period, i.e., one peak below 300 nm (corresponding to Figs. 7 and 8) and another peak at roughly 3 μm. Seldom particles are observed in the size range from 300 nm to 2 μm. In the steady state, the peak below 300 nm is flattened for the GCI and HVOF discs and the particle concentration from 300 nm to 3 μm largely increases.

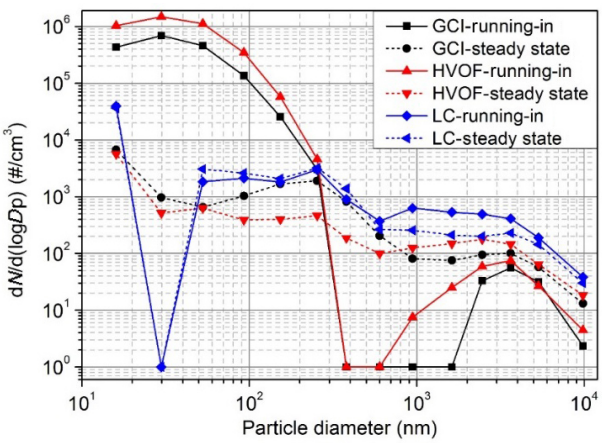

Fig. 9 Particle size distribution obtained using ELPI+.

4 Discussion

4.1 Friction layer characterization

Figure 10 presents the SEM images of the pin worn surface tested against GCI disc. Four regions on the pin worn surface (marked in Fig. 10(a)) were chemically analyzed with EDXS, and the results are listed in

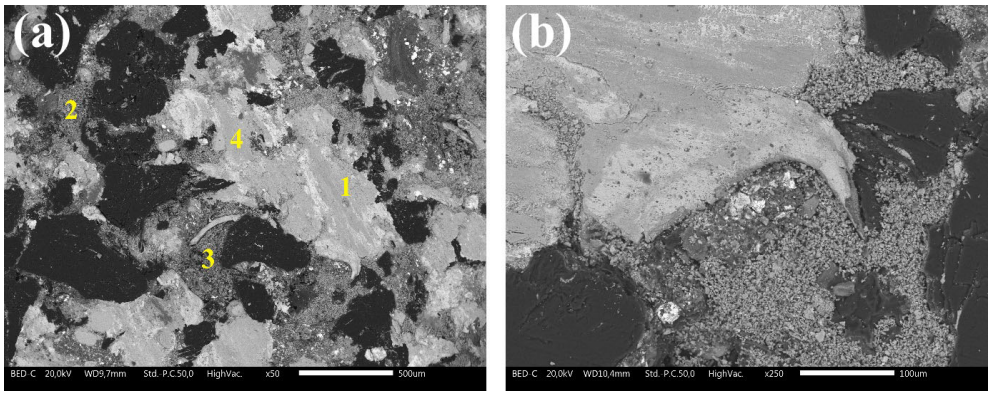

Fig. 10 Backscattered SEM images of pin worn surface tested against GCI disc: (a) the marked four regions, from which EDXS data are obtained and presented in Table 4; (b) typical microstructure of primary and secondary contact plateaus.

Table 4. It can be noted that all the four regions exhibit large content of iron, mainly coming from the tribo-oxidation and transformation from the mating GCI disc. The high concentrations of copper are compliant with the pin composition (Table 1). The typical friction layer composed of primary and secondary contact plateaus is clearly visible in Fig. 10(b), which is in agreement with other literature studies [1, 19, 21, 22]. These plateaus contribute to the stable friction and wear performances of low-metallic brake pad and GCI brake disc contact.

Figure 11 shows the worn surface of the GCI disc, in which four regions were marked and analyzed using EDXS (Table 5). Considering the EDXS results, abrasive grooves (Region 3) and oxidative layers (Regions 1, 2 and 4) are clearly seen in Fig. 11.

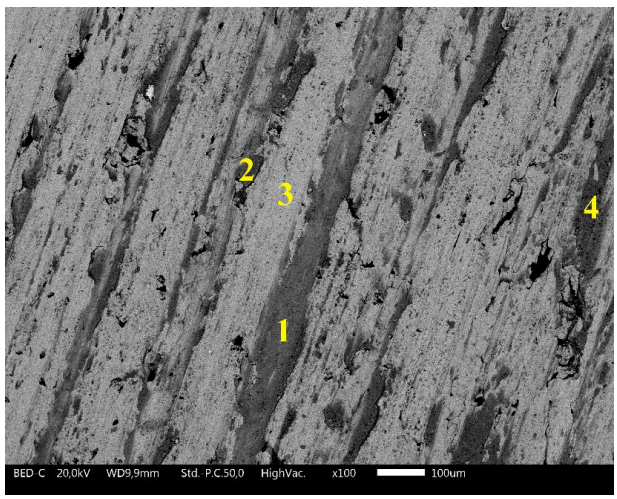

Fig. 11 Backscattered SEM image of GCI disc worn surface. Four marked regions, from which EDXS data are obtained, as presented in Table 5.

Table 4 Chemical composition of four regions from pin worn surface tested against GCI disc detected via EDXS (Fig. 10). Carbon content excluded.

(Unit: wt%)

Region	1	2	3	4
O	20.3	18.6	10.2	24.9
Mg	1.8	1.4	16.4	1.9
Al	0.9	14.2	0.8	1.4
Si	1.2	0.8	—	0.4
S	1.7	1.0	7.1	2.9
Cr	0.9	0.4	1.6	5.6
Fe	24.6	22.6	10.7	33.2
Cu	30.9	21.6	4.6	15.7
Zn	11.8	8.3	14.0	6.7
Sb	4.4	10.3	31.8	6.2
Ba	1.3	0.8	2.8	1.1

Table 5 Chemical composition of four regions from GCI disc worn surface detected via EDXS (Fig. 11). Carbon content excluded.

(Unit: wt%)

Region	1	2	3	4
O	18.9	28.1	3.2	29.0
Mg	1.3	2.2	—	1.3
Al	0.5	0.7	—	0.6
Si	1.4	1.1	1.3	0.7
S	0.8	2.3	—	1.4
Cr	0.2	0.4	0.4	0.5
Mn	0.5	—	0.8	0.4
Fe	68.1	48.9	94.3	45.1
Cu	4.9	8.4	—	12.7
Zn	2.3	4.7	—	4.4
Sb	1.1	3.2	—	3.9

The main mechanisms are abrasive plus oxidative wear, whereas no clear adhesive joint has been observed. The GCI disc worn surface contains several elements transferred from the mating pin, corresponding to the moderate wear rate of the pin, as shown in Fig. 4.

SEM images of pin worn surface tested against HVOF disc are shown in Fig. 12. Three regions which represent typical primary (Regions 1 and 2) and secondary (Region 3) contact plateaus provide the composition data in Table 6. It turns out that the pin worn surface features high concentrations of Cr, Co, and W, all coming from the mating HVOF disc. Some key elements distribution on the pin worn surface are mapped in Fig. 13. The figure indicates that copper is localized in the primary contact plateaus, as reinforcing fibres and carbon are mainly presented as graphite particles. The elements transferred from the HVOF disc (Cr and W) seem to distribute on the entire worn surface except in the graphite.

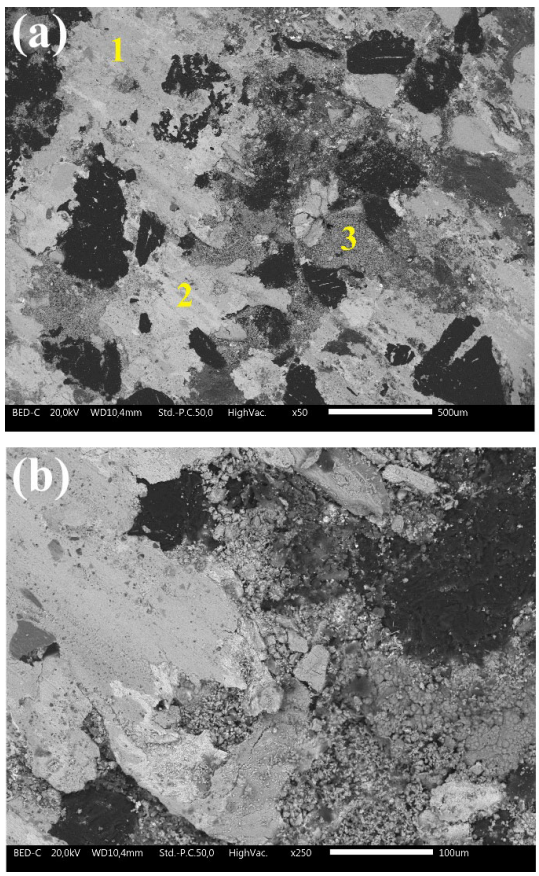

Fig. 12 Backscattered SEM images of pin worn surface tested against HVOF disc: (a) three marked regions, from which EDXS data are obtained, as presented in Table 6; (b) primary and secondary contact plateaus.

Table 6 Chemical composition of three regions detected via EDXS from pin worn surface tested against HVOF disc (Fig. 12). Carbon content excluded. (Unit: wt%)

Region	1	2	3
O	21.3	22.2	24.5
Mg	3.3	4.3	1.6
Al	3.2	2.8	1.0
Si	1.5	2.4	0.5
S	2.3	2.5	2.2
Cr	0.9	0.9	1.4
Fe	10.9	7.2	17.6
Co	0.7	0.8	1.1
Cu	39.3	36.3	18.7
Zn	6.4	8.4	13.6
Sb	4.6	5.3	8.0
Ba	0.9	0.8	1.3
W	4.7	6.1	8.5

The worn surface of the HVOF disc is shown in Fig. 14, in which two main phases are observed, i.e., one light grey phase and one black phase in the backscattered view. Their compositions, measured acquiring EDX spectra in the Regions 1 and 4 in the black phase and Regions 2 and 3 in the light grey phase, respectively, are given in Table 7. The light grey phase has roughly the same composition as the HVOF coating composition (Table 1), whilst the black phase has a high content of Cu and Zn, which are transferred from the mating pin surface. At the same time, Regions 1 and 4 are heavily oxidized, confirming that oxidation is likely to dominate the tribological process.

Although no comparative investigations on the HVOF and LC brake discs can be found in the literature, there are some studies that investigated the differences between the HVOF and GCI brake discs. Jayashree et al. [6] applied similar WC–CoCr coating with HVOF on GCI substrate, and witnessed higher CoF from the HVOF disc than the nude GCI disc, when the contact pressure is higher than 1 MPa, which is corresponding to the CoF results obtained in the current study (Fig. 3). Another study [23] claimed that the higher the contact pressure, the higher the CoF from HVOF sprayed WC–CoCr coating is. This is possibly attributed to the very different chemical

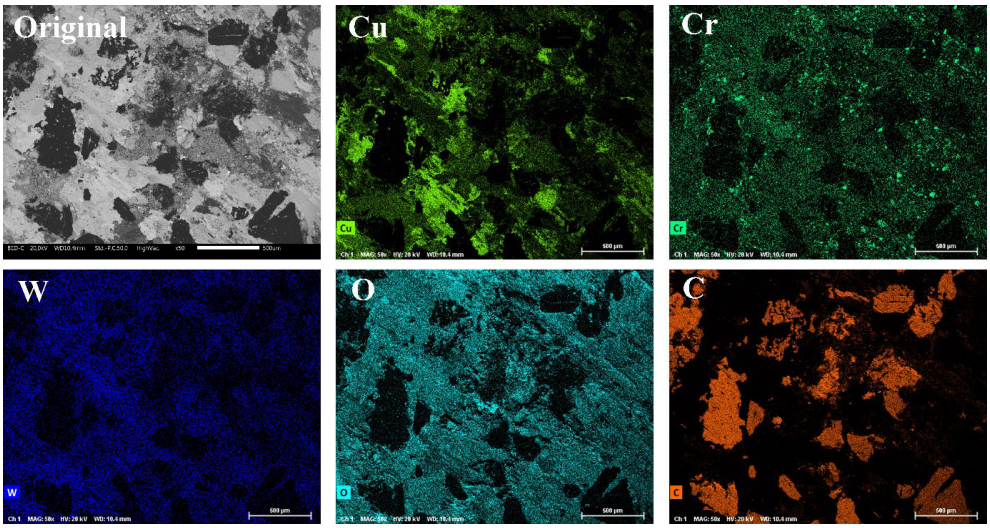

Fig. 13 EDXS mappings showing key elements distribution on pin worn surface against HVOF disc.

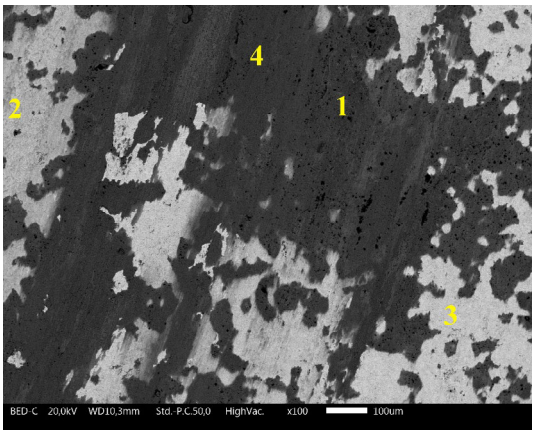

Fig. 14 Backscattered SEM image of HVOF disc worn surface. Four marked regions are chemically analyzed via EDXS, as shown in Table 7.

Table 7 Chemical composition of four regions from the HVOF disc worn surface detected via EDXS (Fig. 14). Carbon content excluded.

(Unit: wt%)

Region	1	2	3	4
O	22.9	18.5	4.1	22.2
Mg	4.5	—	—	2.4
Al	3.9	—	—	1.2
Si	2.8	—	—	1.3
S	2.9	0.9	—	1.8
Cr	1.1	1.8	5.7	1.0
Fe	8.8	1.4	0.7	12.2
Co	—	6.9	6.8	—
Cu	34.8	5.0	—	36.2
Zn	11.3	2.8	—	12.6
Sb	4.3	0.9	—	5.9
W	2.6	61.8	82.7	3.2

composition between HVOF coating and the mating pin. Accordingly, abrasion and oxidation are very likely to dominate the tribological process instead of adhesion. With the increase of contact pressure, the disc surface is rapidly oxidized. The hard tribo-oxides on the disc surface accelerate the abrasive wear of the pin and result in the very high wear rate of the pins tested against HVOF disc (Fig. 4). Meanwhile, the tribo-oxides enhance the ploughing effect, coherently with the reported high CoF (Fig. 3). The high wear rate can also be expected from the pin worn surface shown in Fig. 12(b), in which both the primary and secondary contact plateaus are largely damaged. SEM image of pin tested against LC disc is shown in Fig. 15, in which three regions are analyzed with

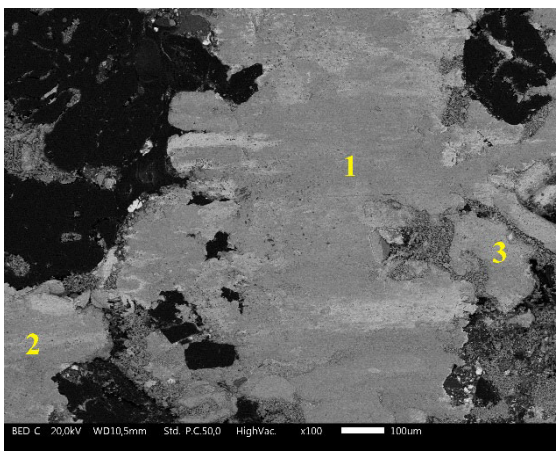

Fig. 15 Backscattered SEM image of pin tested against LC disc. Three marked regions are chemically analyzed via EDXS, as shown in Table 8.

EDXS. All of them present typical composition of contact plateaus (Table 8). The pin worn surface tested with the LC disc is characterized by a high content of Cr and Ni coming from the disc. Its Fe content is comparable to the pin worn surface tested against the GCI disc (Table 4) and notably higher than the pin worn surface tested against HVOF disc (Table 6). The distribution of some key elements on the pin worn surface is also analyzed with EDXS as shown in Fig. 16. It can be seen that Cu and Fe mainly concentrate in the reinforcing fibres, and C only exists in the graphite. Meanwhile, Cr and Ni coming from the mating LC disc are detected on the entire worn surface except the graphite particles.

Table 8 Chemical composition of three regions from pin worn surface tested against LC disc (Fig. 15). Carbon content excluded.

(Unit: wt%)

Region	1	2	3
O	19.2	19.1	17.0
Mg	0.3	1.5	1.0
Al	—	0.9	—
Si	0.3	1.0	0.3
S	1.4	0.9	2.5
Cr	8.2	6.1	6.6
Fe	38.7	28.3	31.9
Ni	1.0	0.8	1.7
Cu	22.1	37.4	23.5
Zn	6.6	3.1	8.9
Sb	1.8	0.9	6.1
Ba	0.4	—	0.5

For the worn LC disc surface, two types of regions are seen under SEM backscattered view, as shown in Fig. 17. Their chemical compositions are evaluated from EDXS data (Table 9). It can be noted that the light grey phase (Region 1 in Fig. 17) exhibits very high content of Fe, Cr, and Ni, comparable to the nominal composition of the LC coating (Table 1). The dark grey phase (Region 2 in Fig. 17) has very similar composition as the contact plateaus on the mating pin surface (Table 8). The LC disc has shown a shorter running-in period than the traditional GCI disc (Fig. 3), in agreement with the results in Ref. [2],

Table 9 EDXS obtained chemical composition of two regions from LC disc worn surface (Fig. 17). Carbon content excluded.

(Unit: wt%)

Region	1	2
O	4.6	21.7
Mg	0.2	2.8
Al	0.4	2.3
Si	1.0	1.8
S	0.3	2.4
K	—	0.4
Ca	—	0.6
Cr	17.5	6.7
Fe	71.9	33.4
Ni	2.6	0.8
Cu	1.1	18.5
Zn	0.4	4.8
Sb	—	3.3
Ba	—	0.5

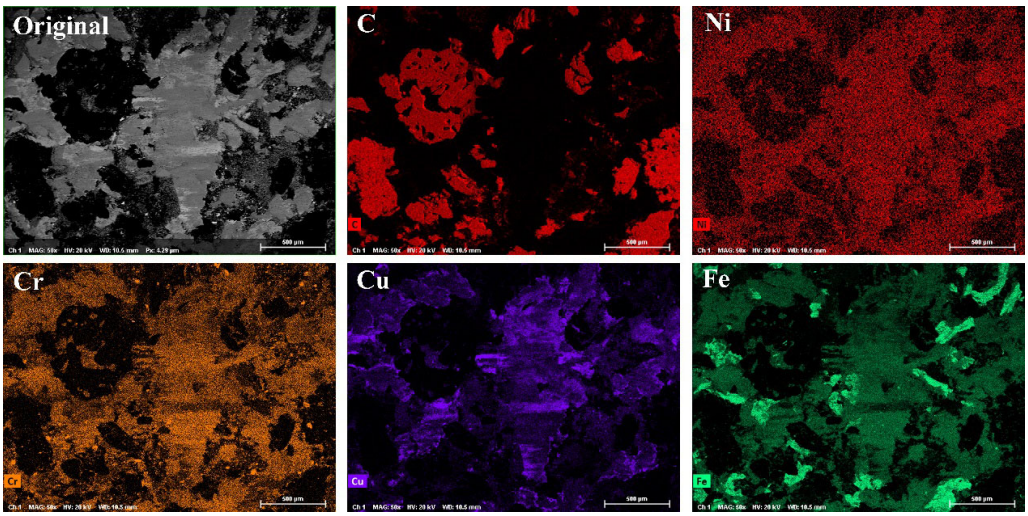

Fig. 16 EDXS mappings showing key elements distribution on pin worn surface against LC disc.

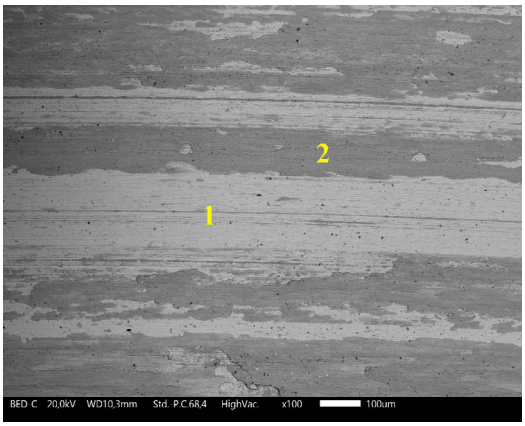

Fig. 17 Backscattered SEM image of LC disc worn surface, showing light and dark gray regions. Two marked regions are chemically analyzed via EDXS, as shown in Table 9.

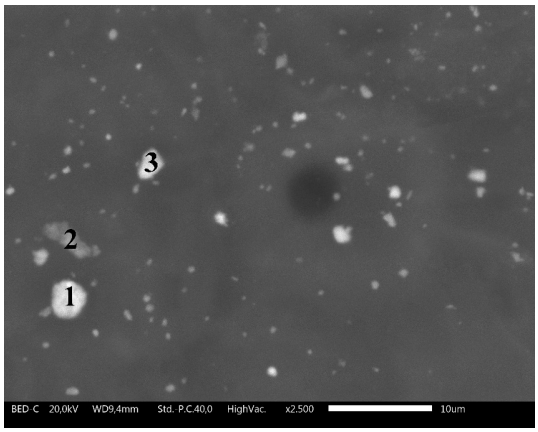

Fig. 18 SEM image of particles generated from pin–GCI pair and obtained from ELPI+ (Stage 5). Three spots are analyzed via EDXS, and results are provided in Table 10.

Table 10 Chemical compositions of three spots marked in Fig. 18. Carbon content excluded. (Unit: wt%)

Spot	1	2	3
O	28.0	40.5	34.2
Mg	5.7	2.7	6.7
Al	2.6	1.1	4.2
Si	1.7	3.3	2.4
P	—	—	1.0
S	2.4	1.1	3.3
Ca	0.3	—	2.5
Cr	0.2	—	0.7
Mn	0.4	—	—
Fe	49.9	42.0	18.6
Cu	0.8	6.2	8.9
Zn	2.2	1.5	11.9
Zr	—	0.4	1.2
Sb	—	1.2	3.0
Sn	2.0	—	—
Ba	3.8	—	1.4

and probably due to the smoother initial surface roughness which makes it easier for the contacting pin and disc surfaces to get conformal with each other. This could also result in the very narrow scatter in the CoF results (Fig. 3). The worn surface of the pins tested with the LC disc (Fig. 15) seems to be more compact than those of the pins tested with HVOF disc (Fig. 12), corresponding to the lower wear rate of the pins tested with LC than the one tested with HVOF disc.

4.2 Particle characterization

The emitted particles from the three brake disc materials, collected on Stage 5 of ELPI+, are also characterized with SEM–EDXS analyses. Of note, the particle size distribution D_{50} of ELPI+ Stage 5 is 94 nm.

The SEM image of the collected particles generated from pin–GCI friction pair is shown in Fig. 18, in which three spots are chemically analyzed with EDXS (results shown in Table 10). It can be seen that part of the collected particles remain alone (the tiny spots in the view), and the others agglomerate into clusters. The appearance of the particles mainly include round, chunky, and flake shapes. Although there is a limitation to clearly increase the magnification further, it can be estimated that the smallest particles collected on this stage are several nanometers.

Figure 19 shows the particles generated from pin–HVOF friction pair and collected on ELPI+ Stage 5. The compositional results coming from the regions 1–4 in Fig. 19 are shown in Table 11. Besides the flake and chunky particles, which are observed in the pin–GCI pair, a large amount of needle-shape particles have been observed for the pin–HVOF pair. Most likely, the needle-shape particles resulted from the abrasive wear of the pin and HVOF disc, are sheared off by the hard WC–CoCr coating materials and tribo-oxide particles. The chemical composition of the particles in Table 11 indicates that the generated particles come from both the pin (e.g., Cu, Zn, Mg, and Al) and the HVOF disc (e.g., Co and W). The smallest particles in the SEM images seem to be several nanometers long in one dimension.

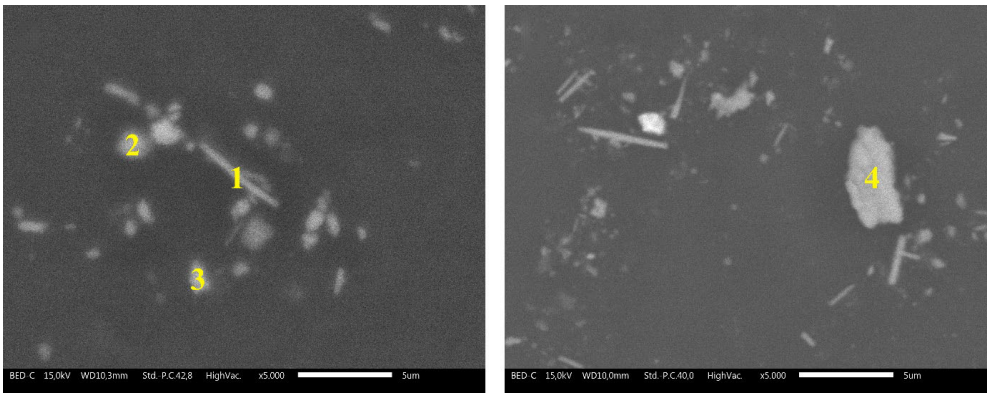

Fig. 19 SEM images of particles generated from pin–HVOF pair and obtained from ELPI+ (Stage 5). Four spots are chemically analyzed via EDXS, and results are shown in Table 11.

Table 11 Chemical compositions of four spots marked in Fig. 19. Carbon content excluded. (Unit: wt%)

Spots	1	2	3	4
O	25.0	26.3	15.5	18.0
Mg	2.8	7.8	4.5	5.5
Al	1.6	5.0	2.6	4.0
Si	0.9	3.4	1.3	—
S	1.2	3.2	2.8	3.8
Cr	0.4	1.7	0.9	2.1
Fe	5.7	19.4	12.1	15.4
Co	—	—	1.2	2.6
Cu	35.0	13.4	35.7	10.9
Zn	17.6	7.3	8.6	4.6
Zr	—	1.7	1.0	6.1
Sb	3.0	4.7	5.1	6.4
Ba	—	1.3	1.5	1.1
W	6.8	4.8	7.2	19.5

The generated particles from the pin–LC friction pair and collected on ELPI+ Stage 5 are shown in Fig. 20, and Table 12 lists the chemical compositions as evaluated acquiring EDX spectra from the three spots marked in Fig. 20. Similarly to the pin–GCI pair, particles in round, chunky, and flake shapes are seen but no needle shapes. The EDXS results in Table 12 confirm the presence of elements from both the pin and LC disc. The particles from pin–LC pair seem to be more heavily oxidized than the particles from pin–HVOF pair (see the O content in Table 11 and Table 12). Combining the coherent tribo-oxide layer observed on the HVOF disc worn surface (Fig. 14), it is thought that the oxides tend to form a layer on the HVOF disc surface, protecting the HVOF disc from severe wear. However, the oxides on the LC disc

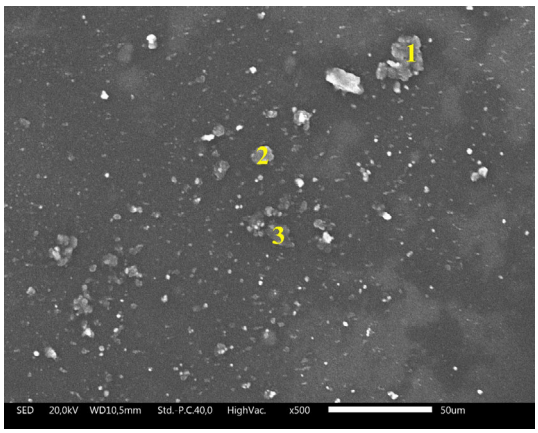

Fig. 20 SEM image of particles generated from pin–LC pair and obtained from ELPI+ (Stage 5). Three spots are chemically analyzed via EDXS, and results are shown in Table 12.

Table 12 Chemical compositions of three spots marked in Fig. 20. Carbon content excluded. (Unit: wt%)

Spots	1	2	3
O	38.7	40.7	53.0
Mg	1.2	1.2	0.5
Al	10.8	11.5	12.8
Si	14.3	14.7	17.9
K	4.4	4.6	4.2
Ca	2.6	4.0	3.7
Ti	1.3	2.1	—
Cr	3.0	2.4	—
Fe	18.4	17.0	3.7
Ni	3.3	—	—
Cu	2.1	1.8	2.2

surface are prone to be crashed into small particles and become airborne.

In the current study, both the running-in period and steady state of the particle number concentration and mass concentration are obtained from the GCI and HVOF discs. Several other studies also addressed similar phenomena concerning these two brake disc materials in both PoD laboratory experiment and full-scale dyno bench tests [19, 24]. Particle concentration and size distribution of the HVOF and LC disc materials in the sub 100 nm range are rarely studied, so that there is little information can be compared. For the GCI discs, particles concentrated between 10 and 80 nm were observed in Ref. [25], similar to the running-in period in the current study (Fig. 8). It should be noted that different contact pressures and sliding speeds will affect the particle size distribution by changing the contact temperature [25, 26], whilst the UFP formation range is always achieved in the pin–GCI brake contact when shifting from mild to severe contact conditions [27]. LC disc presents superior performance as concerns the particle concentration and size distribution in the running-in period, which was neglected in previous studies [2, 3]. Due to the fact that both the brake pad and disc materials will be oxidized in the air, they are probably entitled to a new running-in period after been placed in the open environment after a period of time. Under such circumstances, the LC disc may have better performance than the GCI and HVOF discs, since there is not notably different performance in the running-in period and steady state in terms of (CoF) and particle emissions.

The collected particles from the three friction pairs all contain elements coming from the pin and the disc, confirming the contributions from both components of the tribological pairs. General key elements from the three different friction pairs include O, Mg, Al, Si, Ca, Cr, Fe, and Cu (Tables 10, 11, and 12). Among these, Al, Si, and Cu are not commonly detected in engine exhaust [28] but usually observed in urban environment [29, 30]. Furthermore, Al, Si, and Cu tend to form fine particles and UFP instead of coarse particles [31, 32], and the emitted Cu will finally settle in lake sediments and introduce toxicity to aquatic species [33, 34], which is the motivation of the development of Cu-free brake pad materials [35].

5 Conclusions

A PoD tribometer has been used to investigate the coefficient of friction (CoF), wear rate and ultrafine particle emission from a high velocity oxygen fuel (HVOF) sprayed WC–CoCr coating, a laser cladding sprayed (LC) Fe-based coating, and a traditional grey cast iron (GCI) brake disc material. Wear products, originating from the pin and disc worn surfaces, have been characterized in order to identify the main wear mechanisms dominated the different tribological pair combinations. As concerns the emitted particles, their concentration and size distribution have been measured using a fast mobility particle sizer and an electrical low pressure impactor. Morphology and chemical composition of the emitted particles (impactor stage PM size: D_{50} = 94 nm) are characterized with the scanning electron microscopy and energy dispersive X-ray spectroscopy. Some major conclusions can be drawn from the current study:

1) HVOF disc shows the highest CoF among all the three brake disc materials.

2) LC disc has the shortest running-in period and the most stable performance in the entire test run, in terms of CoF and particle concentration.

3) HVOF disc yields the lowest wear rate, but results in the highest wear to the mating pin. GCI and LC discs have similar wear rate, and lead to similar wear to the mating pins.

4) In the ultrafine particle range, GCI and HVOF discs generate particles mainly concentrating below 100 nm in the running-in period and 200 nm in the steady state. LC disc emits particles constantly concentrating around 200 nm in the entire test run.

5) Brake pad materials tested against GCI and LC discs demonstrate compacted friction layer, but the brake pad material tested against HVOF disc shows largely damaged friction layer.

6) Both the brake pad and brake disc materials transferred to each other during the test. The transferred disc materials homogenously distribute on the pad worn surface expect on the graphite.

7) The appearance of the ultrafine particles from GCI and LC discs mainly include round, chunky, and flake shapes. HVOF disc also emits uniquely needle-shape particles.

8) The generated particles from all the three brake

disc materials are composed of many elements and are largely oxidized. Among these, Al, Si, and Cu are not commonly detected in the engine exhaust particulate matters.

This study raises the awareness of the importance of ultrafine particles emitted from disc brake system, which is considered an important contributor to non-exhaust particle emissions. However, it should be noted that this study only describes qualitative information on the particles on the size boundary around 100 nm. Nanostructure observation and composition analysis on particles in smaller size is needed in future research, especially from the hardfacing coated brake disc materials.

Acknowledgements

The authors are grateful for the financial support from FORMAS: Swedish Research Council for Sustainable Development (No. 2020-02302) (Nescup project). The research also received funding from European Union's Horizon 2020 research and innovation programme (No. 954377) (nPETS project).

References

[1] Lyu Y Z, Ma J J, Åström A H, Wahlström J, Olofsson U. Recycling of worn out brake pads—Impact on tribology and environment. *Sci Rep* **10**: 8369 (2020)

[2] Dizdar S, Lyu Y Z, Lampa C, Olofsson U. Grey cast iron brake discs laser cladded with nickel–tungsten carbide—Friction, wear and airborne wear particle emission. *Atmosphere* **11**(6): 621 (2020)

[3] Olofsson U, Lyu Y, Åström A H, Wahlström J, Dizdar S, Nogueira A P, Gialanella S. Laser cladding treatment for refurbishing disc brake rotors: Environmental and tribological analysis. *Tribol Lett* **69**: 57 (2021)

[4] Abhinav, Krishnamurthy N, Jain R. Corrosion kinetics of Al_2O_3 + ZrO_2·5CaO coatings applied on gray cast iron substrate. *Ceram Int* **43**(17): 15708–15713 (2017)

[5] Menapace C, Mancini A, Federici M, Straffelini G, Gialanella S. Characterization of airborne wear debris produced by brake pads pressed against HVOF-coated discs. *Friction* **8**(2): 421–432 (2020)

[6] Jayashree P, Turani S, Straffelini G. Dry sliding behavior of HVOF WC–CoCr coated counterface against Cu–Sn and SiC–graphite composite materials. *Surf Coat Technol* **397**: 125977 (2020)

[7] Jayashree P, Turani S, Straffelini G. Effect of velocity and temperature on the dry sliding behavior of a SiC–graphite composite against WC–CoCr and WC–FeCrAlY HVOF coatings. *Wear* **464–465**: 203553 (2021)

[8] Federici M, Menapace C, Moscatelli A, Gialanella S, Straffelini G. Pin-on-disc study of a friction material dry sliding against HVOF coated discs at room temperature and 300 ℃. *Tribol Int* **115**: 89–99 (2017)

[9] Federici M, Menapace C, Mancini A, Straffelini G, Gialanella S. Pin-on-disc study of dry sliding behavior of Co-free HVOF-coated disc tested against different friction materials. *Friction* **9**(5): 1242–1258 (2021)

[10] Grigoratos T, Martini G. Brake wear particle emissions: A review. *Environ Sci Pollut Res Int* **22**(4): 2491–2504 (2015)

[11] Piscitello A, Bianco C, Casasso A, Sethi R. Non-exhaust traffic emissions: Sources, characterization, and mitigation measures. *Sci Total Environ* **766**: 144440 (2021)

[12] Thorpe A, Harrison R M. Sources and properties of non-exhaust particulate matter from road traffic: A review. *Sci Total Environ* **400**(1–3): 270–282 (2008)

[13] Schulz H, Harder V, Ibald-Mulli A, Khandoga A, Koenig W, Krombach F, Radykewicz R, Stampfl A, Thorand B, Peters A. Cardiovascular effects of fine and ultrafine particles. *J Aerosol Med* **18**(1): 1–22 (2005)

[14] Kwon H S, Ryu M H, Carlsten C. Ultrafine particles: Unique physicochemical properties relevant to health and disease. *Exp Mol Med* **52**(3): 318–328 (2020)

[15] Garg B D, Cadle S H, Mulawa P A, Groblicki P J, Laroo C, Parr G A. Brake wear particulate matter emissions. *Environ Sci Technol* **34**(21): 4463–4469 (2000)

[16] Olofsson U, Olander L, Jansson A. A study of airborne wear particles generated from a sliding contact. *J Tribol* **131**(4): 44503–44507 (2009)

[17] Wahlström J, Söderberg A, Olander L, Jansson A, Olofsson U. A pin-on-disc simulation of airborne wear particles from disc brakes. *Wear* **268**(5–6): 763–769 (2010)

[18] Lyu Y Z, Leonardi M, Wahlström J, Gialanella S, Olofsson U. Friction, wear and airborne particle emission from Cu-free brake materials. *Tribol Int* **141**: 105959 (2020)

[19] Wahlström J, Lyu Y Z, Matjeka V, Söderberg A. A pin-on-disc tribometer study of disc brake contact pairs with respect to wear and airborne particle emissions. *Wear* **384–385**: 124–130 (2017)

[20] Federici M, Menapace C, Moscatelli A, Gialanella S, Straffelini G. Effect of roughness on the wear behavior of HVOF coatings dry sliding against a friction material. *Wear* **368–369**: 326–334 (2016)

[21] Eriksson M, Bergman F, Jacobson S. On the nature of tribological contact in automotive brakes. *Wear* **252**(1–2): 26–36 (2002)

[22] Filip P, Weiss Z, Rafaja D. On friction layer formation in polymer matrix composite materials for brake applications. *Wear* **252**(3–4): 189–198 (2002)

[23] Vashishtha N, Sapate S G, Gahlot J S, Bagde P. Effect of tribo-oxidation on friction and wear behaviour of HVOF sprayed WC–10Co–4Cr coating. *Tribol Lett* **66**(2): 56 (2018)

[24] Perricone G, Matějka V, Alemani M, Valota G, Bonfanti A, Ciotti A, Olofsson U, Söderberg A, Wahlström J, Nosko O, et al. A concept for reducing PM_{10} emissions for car brakes by 50%. *Wear* **396–397**: 135–145 (2018)

[25] Vojtíšek-Lom M, Vaculík M, Pechout M, Hopan F, Arul Raj A F, Penumarti S, Horák J S, Popovicheva O, Ondráček J, Doušová B. Effects of braking conditions on nanoparticle emissions from passenger car friction brakes. *Sci Total Environ* **788**: 147779 (2021)

[26] Namgung H G, Kim J B, Woo S H, Park S, Kim M, Kim M S, Bae G N, Park D, Kwon S B. Generation of nanoparticles from friction between railway brake disks and pads. *Environ Sci Technol* **50**(7): 3453–3461 (2016)

[27] Tarasiuk W, Golak K, Tsybrii Y, Nosko O. Correlations between the wear of car brake friction materials and airborne wear particle emissions. *Wear* **456–457**: 203361 (2020)

[28] Sharma M, Agarwal A K, Bharathi K V L. Characterization of exhaust particulates from diesel engine. *Atmos Environ* **39**(17): 3023–3028 (2005)

[29] Alves C A, Evtyugina M, Vicente A M P, Vicente E D, Nunes T V, Silva P M A, Duarte M A C, Pio C A, Amato F, Querol X. Chemical profiling of PM_{10} from urban road dust. *Sci Total Environ* **634**: 41–51 (2018)

[30] Borgie M, Dagher Z, Ledoux F, Verdin A, Cazier F, Martin P, Hachimi A, Shirali P, Greige-Gerges H, Courcot D. Comparison between ultrafine and fine particulate matter collected in Lebanon: Chemical characterization, *in vitro* cytotoxic effects and metabolizing enzymes gene expression in human bronchial epithelial cells. *Environ Pollut* **205**: 250–260 (2015)

[31] Lin C C, Chen S J, Huang K L, Hwang W I, Chang-Chien G P, Lin W Y. Characteristics of metals in nano/ultrafine/fine/coarse particles collected beside a heavily trafficked road. *Environ Sci Technol* **39**(21): 8113–8122 (2005)

[32] Kuwayama T, Ruehl C R, Kleeman M J. Daily trends and source apportionment of ultrafine particulate mass ($PM_{0.1}$) over an annual cycle in a typical California city. *Environ Sci Technol* **47**(24): 13957–13966 (2013)

[33] Cui Q, Brandt N, Sinha R, Malmström M E. Copper content in lake sediments as a tracer of urban emissions: Evaluation through a source–transport–storage model. *Sci Total Environ* **408**(13): 2714–2725 (2010)

[34] Shupert L A, Ebbs S D, Lawrence J, Gibson D J, Filip P. Dissolution of copper and iron from automotive brake pad wear debris enhances growth and accumulation by the invasive macrophyte *Salvinia molesta* Mitchell. *Chemosphere* **92**(1): 45–51 (2013)

[35] Straffelini G, Ciudin R, Ciotti A, Gialanella S. Present knowledge and perspectives on the role of copper in brake materials and related environmental issues: A critical assessment. *Environ Pollut* **207**: 211–219 (2015)

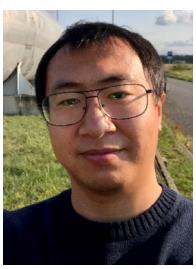

Yezhe LYU. He is an assistant professor in Machine Elements at Lund University (LTH), Sweden. He obtained his Ph.D. degree at KTH Royal Institute of Technology, Sweden, in 2018, with a thesis of *Railway Open System Tribology*. He has been a visiting scientist at Technical University of Darmstadt, Germany within "Future Talent" Programme. He has been awarded the Postdoctoral Fellowship by Japanese Society for the Promotion of Science (JSPS) to visit Keio University. He is the winner of Hakon Hansson Prize of 2021. He is leading and participating several national and international research projects with special research interests on airborne particle emissions in general wear processes and their health and environmental impacts.

Ankur SINHA. He completed his M.S. degree in materials engineering. Currently, he is pursuing his doctoral studies at the Department of Industrial Engineering, University of Trento, Italy. His Ph.D. work aims at developing transmission electron microscopy (TEM) based investigation protocols for fine and ultrafine particulate matter, starting from the non-exhaust vehicular emissions.

Ulf OLOFSSON. He is a professor in tribology at the KTH Royal Institute of Technology, Sweden, since 2006. He received his Ph.D. degree in 1996 on a thesis on wear as failure mechanism in boundary lubricated rolling bearings. He has been a visiting scientist at Sheffield University, UK and at BREMBO SPA Italy. His main research interests include interfaces and especially simulation and prediction of friction and wear, mainly applied to problems in mechanical, automotive, and railway engineering. New research interests include friction modifiers in rolling sliding contacts and joints, airborne particles from wear processes such as in disc brakes and railway wheel to rail contacts.

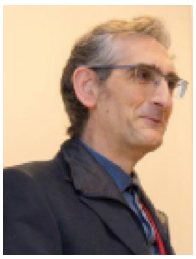

Stefano GIALANELLA. He is an associate professor in materials science and technology. His more recent research interests concern phase transformations, high temperature oxidation and wear of structural alloys and materials for brake systems, nanostructured materials and their microscopy characterization, archaeometry, and cultural heritage issues. On these and related subjects, he teaches courses for undergraduate and graduate students of the Departments of Industrial Engineering and Humanities in the University of Trento, Italy.

Jens WAHLSTRÖM. He is a chaired professor in Machine Elements at Lund University (LTH), Sweden. His research is focused on the tribological performance and non-exhaust emissions from machine elements (such as brakes, gears, and wheel-to-rail) in road and rail vehicles. He has designed and applied both experimental and simulation approaches in his research. He is, and has been, working in several national and international interdisciplinary research projects.